PHYSICAL REVIEW B **89**, 045301 (2014)

# Thermally induced recrystallization of textured hydrogenated nanocrystalline silicon

Giorgia Fugallo[*] and Alessandro Mattoni[†]
*Istituto Officina dei Materiali del CNR (CNR-IOM Cagliari), c/o Dipartimento di Fisica, Cittadella Universitaria, I-09042 Monserrato (CA), Italy*

(Received 18 May 2013; revised manuscript received 26 August 2013; published 6 January 2014)

By an analysis of the local crystallinity based on model potential molecular dynamics simulations we investigated the effect of dissolved hydrogen on the thermally induced recrystallization of nanocrystalline silicon. By using the Kolmogorov-Johnson-Mehl-Avrami theory to analyze the atomistic data, we find that the recrystallization rate decreases exponentially with the hydrogen contamination. At low concentration, the kinetics is moderately affected by the H atoms that tend to migrate to the boundaries increasing their effective interface. At higher H content, we find an increasing number of $\mathrm{Si}_m\mathrm{H}_n$ hydrides that affect the crystalline order of the material and severely impede recrystallization. The analysis based on crystallinity is supported by the atomic scale study of the recrystallization mechanism, here identified as an inverted bond-switching process, and by the ability of hydrates to pin the amorphous-crystalline boundaries.

DOI: 10.1103/PhysRevB.89.045301 PACS number(s): 61.72.−y, 81.10.Jt, 02.70.Ns, 88.40.jj

## I. INTRODUCTION

Nanocrystalline silicon (nc-Si) has attracted considerable interest as an efficient and comparatively low-cost material for third generation thin film solar cells.[1–3] The coexistence in the same texture of nanocrystals and amorphous regions optimally combines the stability against light-induced degradation and the electrical conductivity of the crystalline phase with the red-infrared optical absorption of the amorphous phase.[3] Nc-Si is a complex material with a broad range of different microstructures that can form close to the amorphous-to-crystal phase transformation and whose properties largely depends on the actual intermixing of the two phases.[4,5] The amount of crystalline phase ($\chi$) in nc-Si materials can range from $\chi \sim 1$ in highly crystalline systems (formed by randomly oriented nanocrystals separated by thin grain boundaries) down to $\chi \sim 0.2$ in systems where the more abundant amorphous phase embeds a dispersion of nonaggregated nanocrystals such as spheroid-shaped nanograins[6] (paracrystalline silicon[7]), elongated crystal fibers (textured silicon nc-Si[2]), and many others.

Among several processing issues, hydrogenation (whether intentional or due to contamination) is critical in affecting the electronic properties of nc-Si. High quality films require hydrogen content around 10% (by number of atoms).[8,9] Hydrogen is primarily inserted in order to passivate dangling bonds[8,10] in the amorphous phase and to release microscopic strain,[8,11–13] thus restoring a proper electronic energy gap and reducing the concentration of recombination centers.[14] This enables applications of hydrogenated nc-Si (nc-Si:H) in optoelectronics and photovoltaics through an increased conductivity of photoexcited carriers.[15] In addition, it has been recently demonstrated that hydrogen affects the nature of the electronic localization in the a-Si phase of nc-Si samples and promotes quantum confinement effects.[16] While in that work it is quantified how optoelectronic properties and quantum confinement phenomena in nc-Si are indeed affected by hydrogenation, no information is nevertheless reported about the role of hydrogen on the atomic scale morphology and the microstructure evolution of such a complex material. In particular, hydrogenation is likely to affect the recrystallization kinetics, i.e., the spontaneous transformation from the amorphous to the crystalline phase. Several authors have indicated the importance of hydrogen in nc-Si processed by plasma chemical vapor deposition (PCVD) since it can either promote the formation of nanovoids,[17,18] in a step towards crystallization, or it can simply mediate the transition from amorphous to crystal by interacting with strained Si-Si bonds.[11,19] When hydrogen is dispersed in the film, it affects the relative stability between the amorphous and the crystalline phases and in turn the mobility of the phase boundaries during the solid phase crystallization (SPC) of nc-Si:H (Refs. 20 and 21). Notably, for medium-high concentration (9%–14%), hydrogen is found to reduce the crystalline order of the system[22] slowing down the crystallization.[18] The physics of the recrystallization is complicated because of the morphological complexity introduced by the distribution of crystalline grains and the resulting network of phase boundaries. The Kolmogorov-Johnson-Mehl-Avrami theory (KJMA)[23] provides an analytical correspondence between the crystallinity evolution $\chi(t)$ of the whole system and the mobility of the amorphous crystalline boundary of the individual grains. However, the parameters of the KJMA function (e.g., growth exponent, nucleation time, asymptotic crystallinity) depend on several competing phenomena (e.g., nucleation and growth, interaction between grains) that are difficult to deconvolve without an analysis at the atomic scale.

The atomic-scale understanding of the effect of hydrogen on the microstructure evolution of nanocrystalline silicon is still largely missing. In order to clarify this issue, we performed molecular dynamics (MD) simulations addressed to identify the role of hydrogen on the nc-Si recrystallization phenomena. The theoretical study of this topic is difficult because it requires an accurate description of any relevant atomic scale feature (like, for instance, the local degree of structural order or the hydrogen accumulation), while including a realistic description of the large scale amorphous-crystalline (*a*-*c*) morphology (i.e., the grain size distribution, as well as the network of *a*-*c* interfaces). To this aim, we have taken profit of recent advances in computer modeling of nc-Si and the development of quantitative analysis

©2014 American Physical Society

tools (like, for instance, the local crystallinity).[13,23,24] By the present atomistic simulations, we extend the analysis developed in Ref. 16 and provide evidence that hydrogen at high concentration increases the disorder of the system and it lowers the recrystallization kinetics. The work is organized as follows. After a description of the theoretical framework (Sec. I), we characterize the microstructure evolution of nanocrystalline silicon by varying both the crystallinity and the hydrogen content. In particular, in Sec. II A, we estimate the rate of recrystallization as a function of the hydrogenation and we show that the boundary mobility decreases exponentially with H due to the occurrence of clustering and to the accumulation of hydrides at the boundaries (Sec. II B). In Sec. II C, we study the atomistic details of the elementary recrystallization process investigating the ability of dissolved hydrogen to slow down the mobility of the amorphous crystalline boundaries.

## II. METHODS

Because of the above interplay between atomic- and large-scale features, special care was played in generating our computational samples. We first obtained a set of pure nc-Si systems with different crystal-to-amorphous ratios. To this aim, we quenched from the melt a periodically repeated Si crystal slab formed by $2 \times 50 \times 50$ cubic unit cells, each cell having lateral size 0.54305 nm and containing eight atoms according to the equilibrium density of c-Si. The overall dimension of the system is accordingly $L_x = 1.086$ nm, $L_y = 27.15$ nm, and $L_z = 27.15$ nm) and it contains 40 000 Si atoms. A distribution of isolated grains was then inserted in the amorphous slab by following a twofold procedure; at first, the grains were extracted from a perfect silicon lattice in such a way that their [100] crystallographic direction was parallel to the $x$ direction of the simulation cell; then each grain was randomly rotated around $x$ in order to emulate the experimental regime of casual nucleation and columnar alignment along a preferential direction (texturing). Further details are discussed in Ref. 23. The system was finally thermally annealed at 1200 K for as long as 3 ns. The equations of motion were integrated through the velocity-Verlet algorithm with a time step of 1.0 fs. Temperature was controlled by rescaling atomic velocities. The interatomic forces were calculated according to the environment dependent interatomic potential (EDIP),[25] consisting of two and three-body (angular) terms which both depend on the local atomic coordination. The reliability of such a force field for investigating the microstructure evolution of two-phase Si systems has been established elsewhere,[26] and the crystallization kinetics of mixed *a*-*c* nanosystems has been investigated as well.[23] Because of the annealing, a spontaneous grain growth was observed during the simulations, thus mimicking the real recrystallization process. Three models of nc-Si (hereafter referred to as sample A, B, and C) were obtained by saving the atomic coordinates after 0.05 ns, 1.0 ns, and 3.0 ns of simulated recrystallization, respectively. A cross-section in the $y$-$z$ plane orthogonal to the crystalline fibers of three samples is shown in Fig. 1, By visual inspection of such snapshot configurations, it is easy to extract a qualitative structural characterization. In sample A, the nanocrystals are embedded into the amorphous phase and well separated (i.e., only amorphous/crystalline boundaries are present in the system). Sample B has a larger degree of crystalline order, due to grains of larger diameter. This system contains both *a*-*c* boundaries and grain boundaries. Finally, sample C corresponds to a fully recrystallized system, consisting of large crystalline domains with different crystallographic orientations separated by thin grain boundaries. The three structures are representative of a

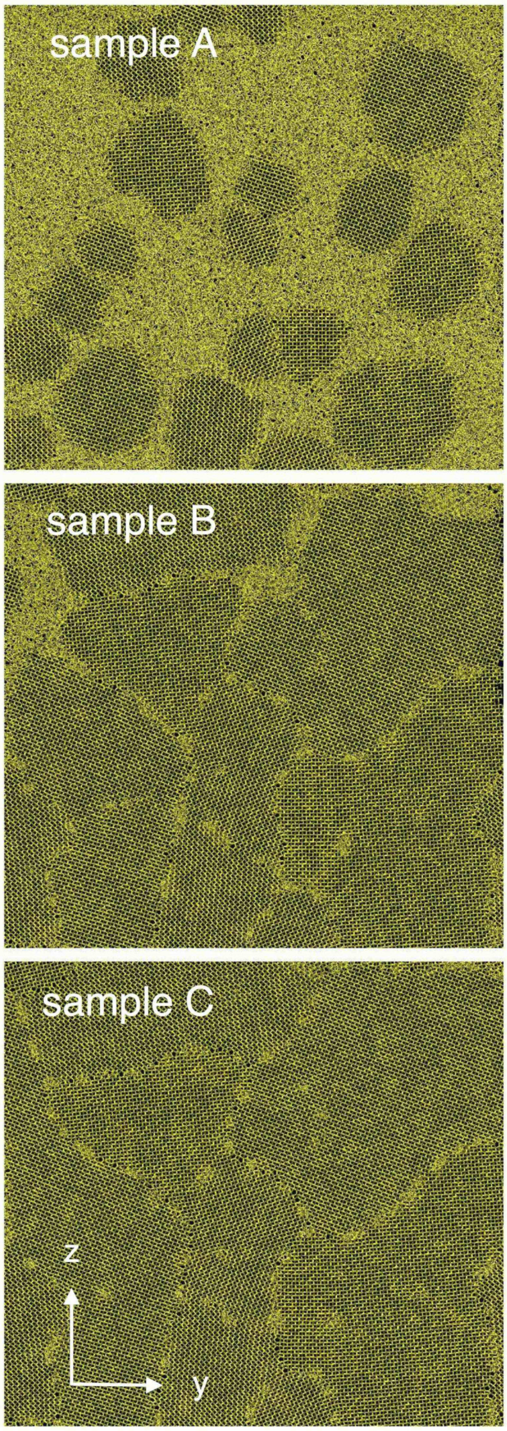

FIG. 1. (Color online) Snapshots of three nc-Si samples: $y$-$z$ planar projection after 0.05 ns (sample A), 1.0 ns (sample B), and 3.0 ns (sample C) annealing time at 1200 K.

wide class of nanocrystalline systems as for the *a-c* ratio and different boundary features.

The investigation of the nc-Si microstructure is performed at two different length scales: (i) at the nanometric scale, we calculated the continuous crystalline phase-field $\chi(y,z)$ through a local analysis of crystallinity, and (ii) at the atomic scale, we have studied the atomic trajectories to clarify the main effects of H on the microstructure evolution.

The key computational tool used to investigate the crystallinity $\chi$ (namely the fraction of atoms forming the crystalline part of the system) is the structure factor (SF), hereafter indicated by $\Theta$. For a system of $N$ atoms,

$$\Theta(t,T) = \frac{1}{N}\left|\sum_{l} e^{i\mathbf{k}\cdot\mathbf{r}_l}\right|, \tag{1}$$

where $r_l$ ($l = 1,\ldots,N$) are the atomic coordinates at time $t$, $\mathbf{k} = (2\pi/d,0,0)$ is set parallel to the columnar $x$-orientated grains,[2,23] and $d$ is the interplanar distance along the [1,0,0] direction. The crystallinity of the sample can be computed from the formula

$$\chi(t) = \frac{\Theta_{ac}(t,T) - \Theta_a}{\Theta_c(T) - \Theta_a}, \tag{2}$$

where $\Theta_c(T)$ and $\Theta_a$ are the SF's calculated (once for all) at the reference temperature for bulk c-Si and a-Si, respectively. For the case of silicon, we calculated a constant $\Theta_a \sim 0.1$ over all investigated temperatures, while $\Theta_c(T)$ was calculated to decrease linearly with increasing temperature from $\Theta_c = 1$ at $T = 0$ K with $1 > \Theta_c > \Theta_a > 0$ for any $T > 0$ and below the c-Si melting temperature, so that the c-Si and the a-Si regions in nanocrystalline samples can be easily identified by calculating the actual value of SF. In order to characterize the local structure within our samples, the simulation cell was divided into a mesh of 1 × 35 × 35 subcells (each containing about 30 atoms). This number is large enough to allow an analysis based on the SF. In fact, for a finite crystal containing $N$ atoms, $\Theta \sim \frac{\sin(Nq/2)}{\sin(q/2)}$, and it converges rapidly to the case of infinite crystal as $N$ increases. The local crystallinity values $\chi_\alpha$ in each subcell $\alpha$ have been interpolated as in Ref. 27, thus obtaining a crystallinity map $\chi(y,z)$ as those reported in Fig. 2. The calculation of the local crystallinity value $\chi_\alpha$ is useful also to identify the phase boundaries (both grain boundaries or *a-c* interfaces). By convention, we set that if locally $\chi_\alpha < 0.3$ ($\chi_\alpha > 0.75$), then that given subcell $\alpha$ is considered to contain amorphous (crystalline) matter. The number of remaining subcells (neither amorphous, nor crystalline) divided by the total number of subcells is a measure of the boundary area, hereafter referred to as effective interface.

## III. EFFECT OF HYDROGEN ON THE MICROSTRUCTURE EVOLUTION

In the first row of Fig. 2, we report the crystallinity maps of samples A (left), B (middle), and C (right), before any hydrogen insertion and thermal annealing: such structures are our starting configurations for the following investigation. Overall, the resulting picture is quite consistent with the previous qualitative structural characterization and it actually provides a quantitative estimate of the different *a-c* ratios in the three samples with total crystallinity of 22%, 87%, and ~91%, respectively.

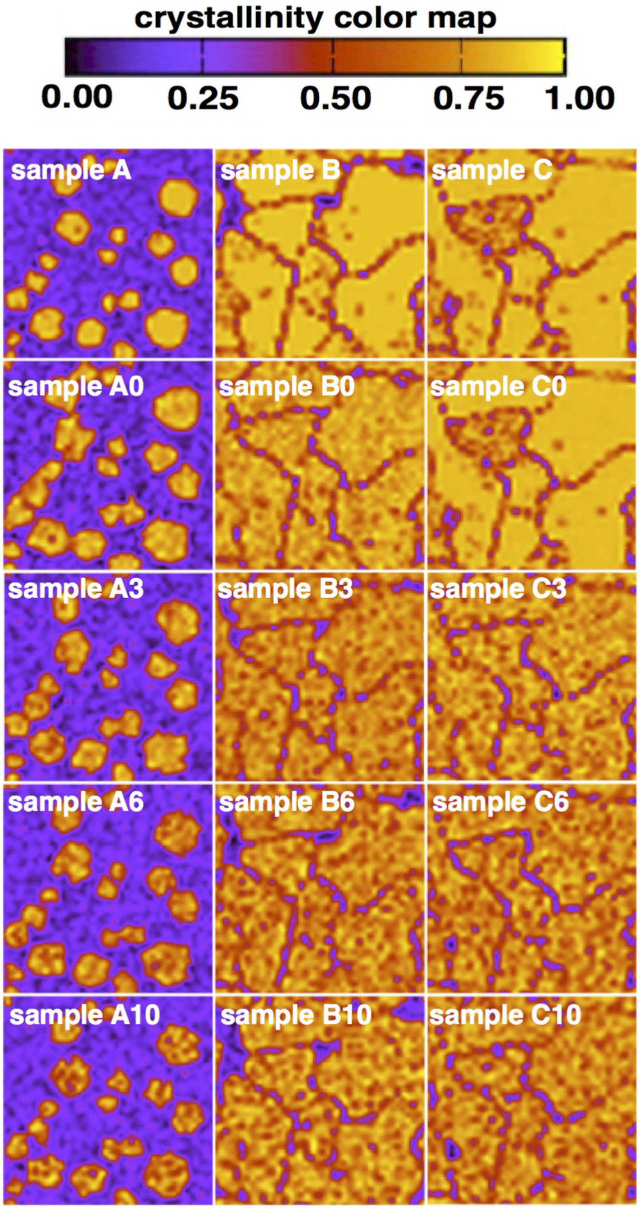

FIG. 2. (Color online) Local crystallinity maps of different $XN$ systems ($X$ = sample A, B, or C; $N$ = 0%, 3%, 6%, or 10% hydrogen content). The first row represents the starting configurations before hydrogenation and annealing. Crystalline and amorphous regions are identified by yellow (light gray) and purple (dark gray) colors, respectively.

In order to study the role of hydrogenation on the microstructure evolution of nc-Si, H atoms were uniformly inserted in samples A, B, and C at three different atomic concentrations (namely, 3%, 6%, and 10%), so generating nine different models of nc-Si:H, hereafter labeled as $XN$, where $X$ identifies the sample (i.e., $X$ = A, B, and C) and $N$ labels the H concentration (i.e., $N$ = 3%, 6%, and 10%). The spatially uniform distribution was obtained by inserting the H atoms at random position within the simulation cell. In order to avoid unphysical initial forces, we rejected those H atoms for which at least one of its nearest neighbor distances was too short (below 0.1 nm). In order to get fully relaxed configurations the systems were relaxed by damped dynamics, i.e., a robust optimization procedure minimizing the product between the force acting on each atom and its velocity that brings the system to a potential energy minimum.

The Si-H interactions in nanocrystalline silicon were described by the Hansen and Vogl (HV) environment-dependent interatomic potential,[28] obtained by combining the Tersoff[29] potential for Si-Si interactions, and the Brenner[30] model for the H-H part. The HV interatomic potential has been extensively validated[31–34] and applied successfully to accurately describe hydrogenated silicon systems[35–37] because it properly accounts for Si-H interactions both in bulk and at silicon surfaces.[28] In order to further establish the reliability of the adopted force field, we investigated the mobility of an isolated hydrogen atom in bulk c-Si and in a-Si, separately. In particular, we evaluated its diffusivity $D(T)$ by calculating the corresponding mean square displacement and we obtained an activation energy for H migration of 0.44 eV (1.34 eV) in c-Si (a-Si). Both values compare well with literature values, respectively ∼0.5 eV and ∼1.5 eV (see Refs. 38 and 39 and references therein).

All samples after hydrogenation (see above) were eventually annealed at $T = 1500$ K for 0.3 ns in order to observe the microstructure evolution features. At this temperature (lower than the melting temperature of the crystalline phase), the thermal mobility of the H atoms in Si is high and the crystallization kinetics is fast. These properties are beneficial in order to reduce the simulation time and so the resulting computational workload. The same annealing procedure was also applied to the H-free samples, so as to directly compare with a microstructure evolution not affected by hydrogenation. In some cases, the calculations have been repeated for systems with double thickness in order to exclude size effects. In particular, we found the same recrystallization mechanism independently on the size of the film (see Sec. II C). The corresponding annealed samples have been labeled as A0, B0, and C0 consistently with the adopted notation.

The crystallinity maps calculated before and after the thermal annealing of both pure and hydrogenated samples are reported in Fig. 2, where each row corresponds to different H content and each column corresponds to a different *a*-*c* ratio of the initial system. We consider first the A system (left column), namely the system with small *a*-*c* ratio. After the annealing and in absence of hydrogen (sample A0) the recrystallization is sizable and the grains grow until some of them are in contact. Conversely, the same grains remain well separated when hydrogen is present, as clearly shown in samples A3, A6, and A10. At the largest H concentration, the grains are practically unchanged with respect to the initial configuration. We conclude that the hydrogen is detrimental for the crystallization, particularly when the concentration is high. Since the annealing time is always the same, the above findings provide evidence that a slower recrystallization kinetics is found when H contamination is larger (see next section). Similar conclusions can be drawn by analyzing the central column of Fig. 2, where the microstructure evolution of sample B is reported. This system has a larger initial value of crystallinity, but there is still a sizable amount of amorphous matter. After the annealing, the amorphous part of the H-free sample B0 has been almost fully recrystallized and only grain boundaries are present. Conversely, in the presence of H, the recrystallization is slower and this is proved by the fact that some amorphous spots are still present after the same thermal annealing. Such effect is larger for larger H content (compare samples B10 and B). Finally, in the case of sample C (right column), containing very little amorphous matter, hydrogen increases structural disorder while its effect on the recrystallization rate is hardly detectable. Overall, the above results show a decrease of the recrystallization rate due the presence of hydrogen contamination.

### A. Rate of recrystallization

In order to support quantitatively the above findings we calculate the velocity of amorphous crystalline boundaries in presence of hydrogen. To this aim, we make use of the Kolmogorov-Johnson-Mehl-Avrami theory (KJMA),[23] which relates the time evolution of the overall crystallinity $\chi(t)$ to that of the individual volume grains $V(t)$. This is in turn a power-law function of time $V(t) \sim (vt)^q$ with $q$ being the growth exponent and $v$ the *a*-*c* boundary mobility, which is the quantity we want to calculate.[23]

In the present analysis, we make use of the KJMA theory in its simplest formulation, i.e., the regime of site saturation occurring when the nucleation time is small and the grains have similar size[23]

$$\chi(t) = \chi_\infty \left\{ 1 - e^{-\pi\rho[v(t+t_0)]^q} \right\},$$

where $\rho = \frac{N}{L_x L_y}$ is the number of grains per area and $\chi_\infty \leqslant 1$ is the asymptotic crystallinity. Here, we have $N = 20$. First of all, we make use of the KJMA to describe the pure silicon recrystallization simulated by the EDIP potential from which samples A, B, and C were extracted. To this aim, we fit the KJMA curve $\chi(t)$ (reported in Fig. 3 as dashed line) passing

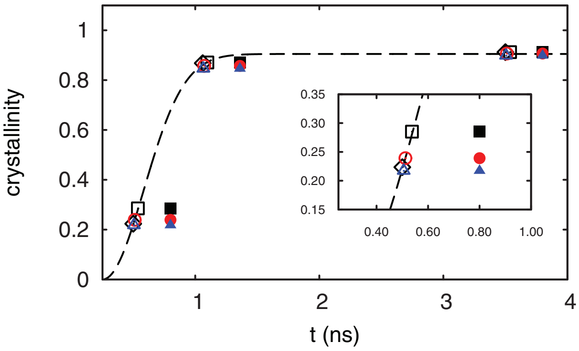

FIG. 3. (Color online) KJMA analytical model of crystallinity $\chi(t)$ (dashed line corresponds to the pure silicon recrystallization according to the EDIP potential) and atomistic data (symbols). Open diamonds correspond to the initial samples A, B, and C. Squares, circles, and triangles correspond to systems at 0%,3%,6% hydrogen, respectively. Filled symbols correspond to annealed systems (by the HV potential adopted in this work), while empty symbols are obtained after rescaling. Inset shows the case of A samples.

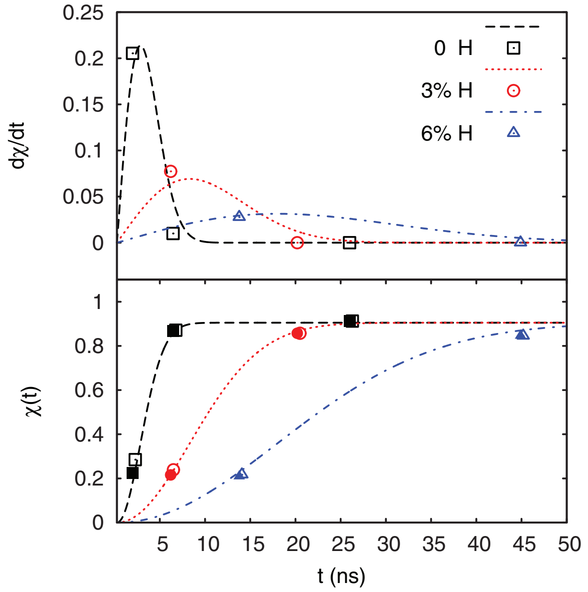

FIG. 4. (Color online) Crystallinity evolution $\chi(t)$ (bottom) and rate of recrystallization $\frac{d\chi}{dt}$ (top) of hydrogenated silicon simulated by the HV model for different hydrogen content. Squares, circles, and triangles (atomistic data) and dashed, dotted and dot-dashed curves (fitting models) correspond to 0%, 3%, and 6% hydrogen, respectively.

on the empty diamonds at points (0.5 ns, 0.22), (1.06 ns, 0.87), and (3.5 ns, 0.91) corresponding to the initial nonhydrogenated systems A, B, and C, respectively. The fitted parameters are $\chi_\infty = 0.905$, $q = 2.02$ (consistent with an interface limited growth[23]), and $v = 7.4$ m/s (also referred to as $v^{\mathrm{ref}}$). The crystallinity of hydrogenated systems after the 0.3 ns long annealing (simulated by the HV force field adopted in the present work) correspond to filled symbols (0%, 3%, and 6% correspond to squares, circles, and triangles, respectively) displaced in $t$-$\chi$ plane by vectors ($\Delta t = 0.3$ ns, $\Delta\chi_X^H$). In particular, the crystallinity increments $\Delta\chi_X^H$ upon annealing depend on both the sample crystallinity $X$ and the hydrogen content $H$.

The important result is that up to 6% hydrogenation the same KJMA functional form describes the recrystallization of the hydrogenated systems, provided that the velocity is suitably rescaled $\chi(v^{\mathrm{ref}} t) \to \chi(f^H\, v^{\mathrm{ref}} t)$ by a constant $f^H$ only dependent on hydrogen content. This is shown in Fig. 3 where filled (empty) symbols refer to data before (after) the rescaling. $f^H$ provides a direct measure of the velocity with respect to the reference EDIP crystallization ($v^H = f^H\, v^{\mathrm{ref}}$) and it can be calculated from atomistic data as

$$f^H \simeq \frac{\Delta\chi_X^H}{\Delta t} \bigg/ \frac{d\chi}{dt}(X).$$

The recrystallization kinetics $\chi(t)$ calculated at 0%, 3%, and 6% H content is reported in Fig. 4 (bottom panel) together with the rate of recrystallization $\frac{d\chi}{dt}$ (top panel). According to KJMA functional form, the crystallinity monotonically increases up to asymptotic limit $\chi_\infty$, while the rate increases up to a maximum value and then decreases to zero at long annealing time when the systems are largely crystalline. By increasing the H concentration from 0% to 6%, the time scale for recrystallization increases by almost one order of magnitude.

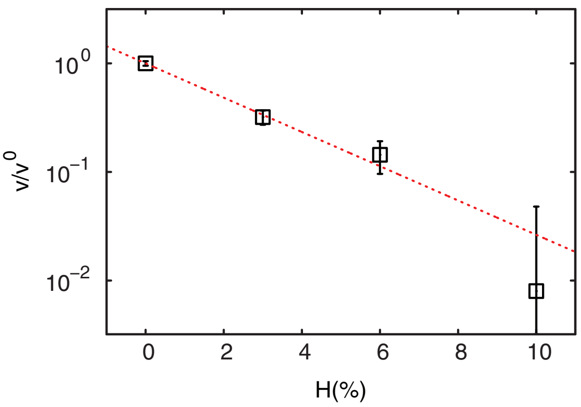

FIG. 5. (Color online) Crystallization velocity as a function of hydrogen content.

The main conclusion of this analysis is reported in Fig. 5 where the $a$-$c$ boundary velocity $v^H$ is shown as a function of H content. Velocities are normalized to $v^0$ (i.e., solid phase recrystallization in the nonhydrogenated case) for which we get $v^0 = f^0 v^{\mathrm{ref}} \sim 0.9$ m/s a value that is one order of magnitude smaller ($f^0 = 0.125$) than in the EDIP case $v^{\mathrm{ref}}$ (corresponding to curve of Fig. 3), this latter value already known to be largely overestimated.[40] Conversely, the present Tersoff value $v^0$ can be considered in reasonable agreement with experimental data. In fact, for macroscopic thicker systems at the same temperature, the recrystallization velocity is of the order of several centimeters per second (see Ref. 40) and similar values are obtained from $v^0$ by taking into account the absence of stress[26] and a factor dependent on film width $v \sim \frac{L_x}{L_0}$ (see Ref. 24) with $L_0$ intrinsic roughness $L_0 \sim 10$ nm measured in $a$-$c$ boundaries.[41] As for the hydrogenated case, the velocity as a function of H (see Fig. 5) can be fitted by an exponentially decaying function confirming the detrimental effects of hydrogen on crystallization discussed above. At 6% H content, the velocity is reduced by a factor 5 with respect to the pure silicon case. It is important to remark that the severe reduction of crystallization kinetics is not related to strain effects due to H insertion. In fact, it has been shown both theoretically and experimentally[26,42] that the amorphous-to-crystal transformation involves an in-plane expansion in the direction normal to the interface and the growth rate is expected to increase under hydrostatic compression. In the systems investigated in this work, the insertion of H atoms induce a small compressive strain consistent with experiments[43] (0.35%,0.42%,0.5% at 3%,6%,10% H content, respectively) so that an enhancement of growth rate is expected. Conversely, our atomistic results show the opposite trend and this is a proof that the H-induced slowing down of kinetics is not due to strain effects.

### B. Hydrogen distribution, clustering phenomena, and disorder increase

It is interesting to study the effect of thermal annealing on distribution of hydrogen atoms. The isolated hydrogen atoms

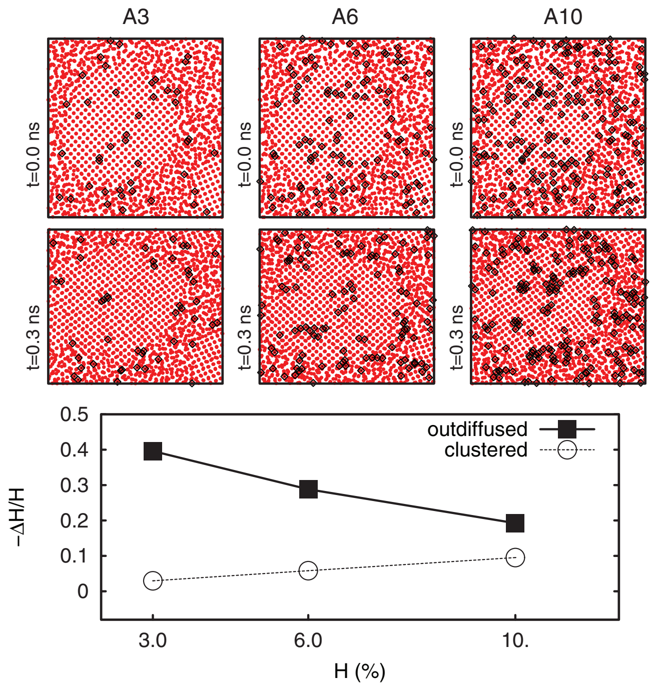

FIG. 6. (Color online) (Bottom) Fraction $-\Delta H/H$ per unit of crystalline phase of out-diffused H atoms (filled symbols) and clustered H atoms (empty symbols) within the crystalline phase as a function of the initial H concentration. (Middle and Top) Portion of sample A before (top) and after (bottom) annealing at the three H concentrations (left, middle, right corresponding to 3%, 6%, and 10%, respectively).

tend to out-diffuse from the crystalline phase (where the H diffusivity is higher[38]) to the amorphous phase (where H is less mobile). This effect is investigated in the samples with low crystallinity, namely, A3, A6, and A10. Filled squares (in the diagram of Fig. 6) give the fraction of escaped H atoms per unit of crystalline phase $-\Delta H/H$ as a function of the initial hydrogenation $H$. The calculated values are positive $-\Delta H/H > 0$ confirming the tendency of hydrogen to escape from the grains. The strongest effect observed at 3% H for which a large fraction of H (0.40) migrate to the boundaries after annealing. The fraction decreases down to 0.2 at 10% H content. Such a reduction is due to the formation of less mobile H aggregates within the crystalline phase. In fact, the number of clustered hydrogens increases with $H$ as can be predicted by a uniform distribution where the fraction of clusters $\rho_c$ is $\rho_c = 1 - e^{-H}$ (see open symbols in bottom panel of Fig. 6).

The clustering effect is clearly observable in the atomic distribution (middle and top panels of Fig. 6) reporting the same portion of system A before (top) and after (bottom) annealing at the three H concentrations (left, middle, right corresponding to 3,6,10%, respectively). Silicon and H atoms are represented as red circles and black diamonds, respectively. In particular, for A3, the grain after annealing is almost hydrogen free with H atoms accumulated at the cylindrical grain boundary (except for a dimer and an isolated hydrogen still in the grain). At higher hydrogen concentrations (A6 and A10), there is a larger number of H aggregates that cannot out-diffuse and the amount of residual H within the grain increases.

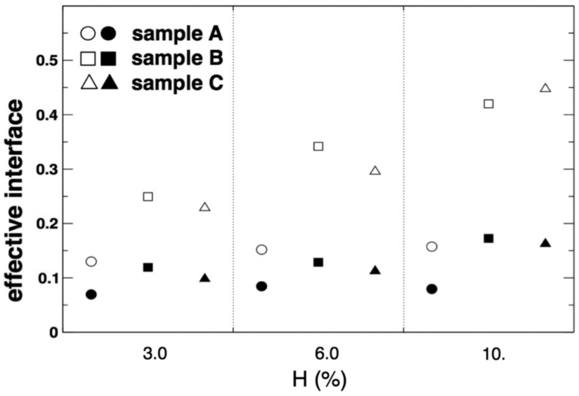

FIG. 7. Effective interface versus hydrogen content before (filled symbols) and after (empty symbols) annealing.

The above tendency of hydrogen atoms is observed also in the cases of samples B and C. This diffusive phenomenon has also implications on the microstructure of the boundaries. This is particularly evident in the case of sample C (right column of Fig. 2), containing very little amorphous matter. H affects the thickness of the grain boundaries, namely, the higher is the H content, the larger is the effective interface. At the same time, an increase of the atomic scale disorder of the grains due to clusters is found (see C10).

The effect on the interfaces is demonstrated quantitatively in Fig. 7 where the effective interface as a function of the H concentration is reported before (filled symbols) and after (empty symbols) the annealing for the sample A (circles), B (squares), and C (triangles). In any case we observe that the higher is the H occurrence the larger is the increment of the interface area after annealing. We finally observe that for a given value of H content, the interface area has a larger increment in samples B and C than in sample A. This can be explained since they have a larger crystalline fraction and, therefore, a larger amount of H that can diffuse easily to the boundaries.

### C. Effects of hydrogen clustering on the atomic-scale recyrstallization mechanisms

The picture outlined so far provides evidence that the recrystallization kinetics slows down at high H contamination. To better clarify the nature of H clusters and its effect on the microstructure evolution, we analyze the microscopic recrystallization mechanism. In Fig. 8, a portion of sample A is reported (middle panel) during recrystallization. Two rectangular regions in the $y$-$z$ cross-section are selected within the system, one at the crystal-amorphous boundary (yellow frame) and the second within the amorphous phase (white frame). The two selections are magnified in the right and left panels, respectively, where only two atomic planes have been represented for clarity. Red (yellow) spheres represent hydrogen (silicon) atoms.

The analysis of these regions confirms a sizable precipitation phenomenon associated to the presence of H, and we can

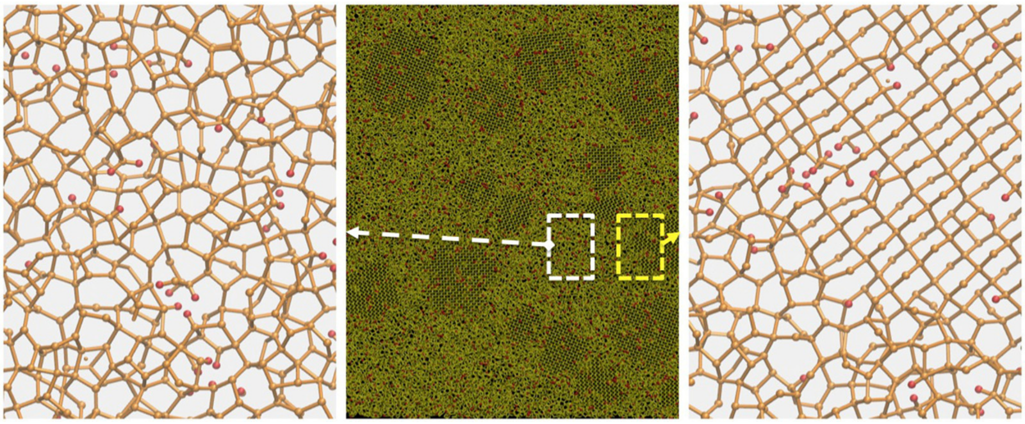

FIG. 8. (Color online) Nc-si at 10% hydrogen content (sample A10) (middle); SiH clusters can be observed both the amorphous (left) and crystalline (right) regions of the system.

better clarify the nature of H clusters in the formation of $Si_nH_m$ hydrides and mono- and divacancies. Furthermore, complexes involving H atoms are found in both crystalline and amorphous phases. In the amorphous phase, the main role of hydrogen is to passivate Si dangling bonds by forming Si-H bridges (see left panel of Fig. 8). Pairs of Si-H are likely to aggregate into silicon nanovoids where the two hydrogen atoms are connected to second-neighbor silicon atoms (several examples occurs within the amorphous region reported in right panels). Pairs of H atoms can also form $SiH_2$ hydrides (an example occurs in the central region of left panel). Larger aggregates of H atoms are also possible. For example, a cluster containing five hydrogens can be observed in the left panel. Notably, Si-H aggregates are found in the crystalline phase, as well (see Fig. 8, right panel). Most of H atoms within the crystalline regions are isolated and passivate the silicon dangling bonds but some larger $Si_nH_m$ hydrides are found as well (e.g., $SiH_2$, $SiH_3$). During the annealing, the small clusters tend to aggregate within the crystalline phase into larger less mobile structures so forming highly disordered regions within the crystals. These results for the nc-Si/a-Si:H systems are in agreement with previous literature[44] on the a-Si:H microstructure, reporting an inhomogeneous distribution of H atoms where few isolated H atoms, monohydrides and dihydrides occur in both sparse and clustered environment. Furthermore, at H concentration around 10%, we observe clusters formed by 4–5 H atoms whose dimension further increases (up to 20 H atoms) at hydrogen content beyond 20%. This is consistent with previous findings[44] in a-Si:H.

The formation of SiH aggregates has an impact on the microstructure evolution of nanocrystalline silicon. First of all, the H aggregation decreases the crystalline order within the grains. This can be proved by an analysis of the crystallinity maps of hydrogenated nc-Si with respect to ideally pure nc-Si. Let us consider the sample A and focus on the largest crystalline region (bottom right corner of panel labeled A of Fig. 2). Upon annealing, the crystallinity of this grain is practically unaffected, provided that no hydrogen is present, as clearly shown in panel A0 of the same figure. At variance, the crystallinity value remarkably decreases when H is present and the larger is the hydrogen amount, the larger is such an effect. The amorphous spots appearing within the grain correspond to a sizable local reduction of the crystalline order due to the formation of $Si_nH_m$ hydrides.

Beside inducing disorder, hydrogen affects the recrystallization process by lowering the mobility of the $a$-$c$ boundaries already analyzed in the previous sections. Figure 9 shows the microstructure evolution (during 0.5 ns long annealing at 1200 K) of the same portion of nanocrystalline silicon (the one reported in right panel of Fig. 8) at 10% H (bottom) or in the pure silicon case (top). We have chosen a portion of the system such that a sizable recrystallization occurred in presence or absence of hydrogen. In the thin cross-section of the system reported in Fig. 9, it is possible to distinguish the amorphous and the crystalline phase. This latter is characterized by the periodic pattern consisting of rectangular cells. Accordingly, the amorphous-crystal interface corresponds to the network of cells at the crystal borders (light gray shadowed). After thermally induced grain growth (right panels), new crystalline cells are formed in the system (Fig. 9, gray dark shadowed). Since the annealing time is the same for the two cases, the number of recrystallized cells provides a rough estimate of the local recrystallization kinetics. In particular, we found locally a smaller number of recrystallized cells in the hydrogenated case (bottom) with respect to pure silicon (top) corresponding to a local deceleration factor $v^H/v^0$ around 4 : 10. This reduction is consistent with the global velocity reduction reported in Fig. 5 taking into account that in the local area (about 1/100 of the whole system) the H concentration deviates from the average value.

The slower dynamics is due to the presence of H atoms (the only difference between the top and bottom cases). To better clarify this point, we focus first of all on the crystallization mechanisms the pure silicon case (top). We identify the simplest mechanism as sequence of events of forming-breaking bonds among triplets of atoms. An example is reported in Fig. 9 (top) for the triplet of atoms labeled by 1, 2, and 3. By labeling $(i-j)_a$ and $(i-j)_c$, the bonds between $i$ and $j$ atoms within the amorphous or the crystalline phase, respectively, we can describe the recrystallization as

$$\begin{aligned}(1-2)_a(2-3)_a &\rightarrow (1-2)_a(2-3)_a(3-1)_a\\ &\rightarrow (2-3)_c(3-1)_c.\end{aligned}$$

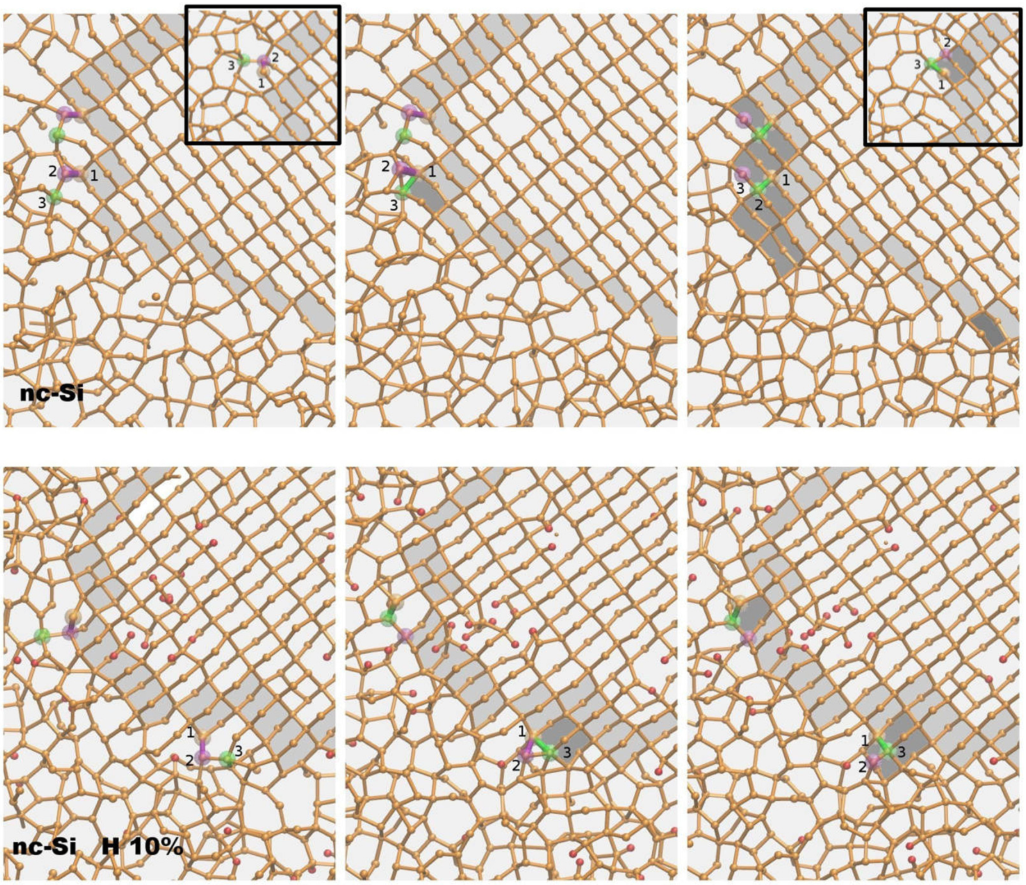

FIG. 9. (Color online) Mechanisms of recrystallization of textured nanocrystalline silicon without hydrogen (top row) and 10% hydrogen (bottom row) observed during 0.5 ns annealing at 1200 K. Insets show the same recrystallization mechanism in a thicker sample of width $2.5L_x$.

The mechanism is shown in Fig. 9: the initial 1-2 bond (purple) breaks and the 3-1 bond (green) forms, with an intermediate step in which the three bonds $(1-2)_a(2-3)_a(3-1)_a$ coexist. The bond occurs when two atoms fall below the cutoff distance of the interatomic potential (3.0 Å for the Si-Si case). At the end of the recrystallization reaction the three atoms belong to the boundary of the crystalline phase. The reaction is a bond switch since it does not change the total number of bonds and it can be considered as the reversal of the WWW[45] algorithm, which is used to generate a perfect four-fold coordinated amorphous silicon from the crystal phase. This recrystallization mechanism is independent on the size of the system and it has been also identified in the nc-Si samples with 2.5 times larger thickness (see top insets in Fig. 9). As for the rate of recrystallization in thicker systems, it is expected to see a reduction, which in fact is observed. In the case of hydrogenated nanocrystalline samples (bottom rows), the same crystallization reactions can be still observed in the H-free regions of the system. The qualitative difference with respect to the nonhydrogenated cases is that $Si_nH_m$ aggregates affect the silicon bond network and inhibit locally the crystallization switch so pinning the *a*-*c* boundary. In bottom panel of Fig. 9, a large Si-H cluster containing up to nine hydrogen atoms form during the annealing (compare left and right panels) and its presence prevents the recrystallization otherwise occurring in the pure silicon (top row of Fig. 9). The cluster is formed during the annealing by the aggregation of smaller moieties ($SiH_2$, SiH, $Si_2H_2$, $SiH_3$) that eventually aligns in the $\langle 110\rangle$ direction while diffusing within the grain towards the *a*-*c* boundary. At variance with aggregation, the complete dissolution of SiH clusters into isolated H atoms has never been observed during the dynamics indicating that the clustering is the dominant phenomena and that SiH clusters persists in recrystallized system with larger abundance at the grain boundaries. Break-up of the clusters is expected to occur over much longer time scale with respect to aggregation (occurring at the nanosecond scale) similarly to what was observed for silicon-boron clusters during the solid phase epitaxy of amorphous silicon-boron[46,47] or in silicon-carbon systems.[48,49] Overall, the present analysis clearly supports the slowing of the crystallization kinetics of nanocrystalline silicon as a result of the presence of H previously dispersed in the nc-Si sample. Present theoretical results are nicely consistent with the observation that H accumulates at the interface[21] and, more important, to the fact that high H content in nc-Si films introduces structural disorder[22] impeding the growth of large grains[50,51] with a resulting inhibition of the crystallization process.[9,18] In particular the formation of Si-H aggregates and their accumulation at the c-Si/a-Si:H boundaries can explain the calculated reduction of boundaries mobility, and the larger activation energy for recrystallization observed[9] in nc-Si films when hydrogen is inserted. Nevertheless, we note that the present scenario does not necessarily apply to the case of a nc-Si treated by a hydrogen plasma, for which, at variance with our investigation, hydrogen atoms provide additional energy with respect to average thermal budget and they can even activate and enhances the recrystallization.[11,19]

## IV. CONCLUSION

In conclusion, by means of model potential molecular dynamics simulations we studied atomic scale mechanisms of recrystallization in a model of textured nanocrystalline silicon and we provided evidence that hydrogen by inducing local structural disorder and clustering phenomena impedes the full recrystallization of mixed-phase amorphous/crystalline silicon systems consistently with experiments on solid phase crystallization. This effect is enhanced by increasing the H content with a recrystallization rate that decreases exponentially with H concentration. In particular, we find that at low concentration the hydrogen tends to migrate from the crystal phase to amorphous one directly affecting the thickness of the grain boundaries and increasing their effective interface. At higher concentration an increasing large fraction of hydrogen precipitates into immobile $\mathrm{Si}_n\mathrm{H}_m$ hydrides (similarly to the case of a-Si:H) affecting the crystalline order of the system and further impeding recrystallization.

## ACKNOWLEDGMENTS

We acknowledge L. Colombo (Department of Physics, University of Cagliari) for critical reading of the manuscript and M. Lusk and L. Bagolini (Colorado School of Mines, USA) for useful discussions. A.M. acknowledges financial support by Istituto Italiano di Tecnologia (IIT-SEED POLYPHEMO and “Platform Computation”), Regione Autonoma della Sardegna (L.R. 7/2007 CRP 18013 and CRP-249078), MIUR (Project PON-NETERGIT), and CNR (Project Premialità RADIUS).

---

[*] Present address: IMPMC, Université Pierre et Marie Curie, CNRS, 4 place Jussieu, F-75252 Paris, France; giorgia.fugallo@impmc.jussieu.fr

[†] Corresponding author: mattoni@iom.cnr.it

[1] O. Morton, Nature (London) **443**, 19 (2006).

[2] S. Pizzini, M. Acciarri, S. Binetti, D. Cavalcoli, A. Cavallini, D. Chrastina, L. Colombo, E. Grilli, G. Isella, M. Lancin *et al.*, Mat. Sci. Eng. B **134**, 118 (2006).

[3] O. Vetterl, F. Finger, R. Carius, P. Hapke, L. Houben, O. Kluth, A. Lambertz, A. Mück, B. Rech, and H. Wagner, Sol. Energy Mater. Sol. Cells **62**, 97 (2000).

[4] C. Spinella, S. Lombardo, and F. Priolo, J. Appl. Phys. **84**, 5383 (1998).

[5] F. Cleri and P. Keblinski, Int. J. Comp. Sci. Eng. **2**, 242 (2006).

[6] M. R. Bergren, B. J. Simonds, B. Yan, G. Yue, R. Ahrenkiel, T. E. Furtak, R. T. Collins, P. C. Taylor, and M. C. Beard, Phys. Rev. B **87**, 081301 (2013).

[7] P. M. Voyles, J. E. Gerbi, M. M. J. Treacy, J. M. Gibson, and J. R. Abelson, Phys. Rev. Lett. **86**, 5514 (2001).

[8] G. Lucovsky, G. Parsons, D. Zeller, K. Wu, B. Papas, J. Whitten, R. Lujan, and R. A. Street, J. Optoelect. Adv. Mat. **13**, 1586 (2011).

[9] E. Math, A. Naudon, M. Elliq, E. Fogarassy, and S. de Unamuno, Appl. Surf. Sci. **54**, 392 (1992).

[10] J. Tauc, R. Grigorovici, and A. Vancu, Phys. Status Solidi (B) **15**, 627 (1966).

[11] S. Sriraman, S. Agarwal, E. S. Aydil, and D. Maroudas, Nature (London) **418**, 62 (2002).

[12] P. A. Khomyakov, W. Andreoni, N. D. Afify, and A. Curioni, Phys. Rev. Lett. **107**, 255502 (2011).

[13] L. Bagolini, A. Mattoni, and L. Colombo, Appl. Phys. Lett. **94**, 053115 (2009).

[14] B. M. George, J. Behrends, A. Schnegg, T. F. Schulze, M. Fehr, L. Korte, B. Rech, K. Lips, M. Rohrmüller, E. Rauls *et al.*, Phys. Rev. Lett. **110**, 136803 (2013).

[15] X. C. R. Zhang and H. Wu,Appl. Phys. Lett. **94**, 242105 (2009).

[16] L. Bagolini, A. Mattoni, G. Fugallo, L. Colombo, E. Poliani, S. Sanguinetti, and E. Grilli, Phys. Rev. Lett. **104**, 176803 (2010).

[17] C. Godet, N. Layadi, and P. R. i Cabarrocas, Appl. Phys. Lett. **66**, 3146 (1995).

[18] K. Sharma, M. A. Verheijen, M. C. M. van de Sanden, and M. Creatore, J. Appl. Phys. **111**, 033508 (2012).

[19] R. A. Street, Phys. Rev. B **43**, 2454 (1991).

[20] G. L. Olson and J. A. Roth, Mat. Sci. Rep. **3**, 1 (1988).

[21] L. Xu, Z. P. Li, C. Wen, and W. Z. Shen, J. Appl. Phys. **110**, 064315 (2011).

[22] A. H. Mahan, B. Roy, J. R. C. Reedy, D. W. Readey, and D. S. Ginley, J. Appl. Phys. **99**, 023507 (2006).

[23] A. Mattoni and L. Colombo, Phys. Rev. B **78**, 075408 (2008).

[24] A. Mattoni and L. Colombo, Phys. Rev. Lett. **99**, 205501 (2007).

[25] J. F. Justo, M. Z. Bazant, E. Kaxiras, V. V. Bulatov, and S. Yip, Phys. Rev. B **58**, 2539 (1998).

[26] N. Bernstein, M. J. Aziz, and E. Kaxiras, Phys. Rev. B **61**, 6696 (2000).

[27] A. Mattoni, L. Ferraro, and L. Colombo, Phys. Rev. B **79**, 245302 (2009).

[28] U. Hansen and P. Vogl, Phys. Rev. B **57**, 13295 (1998).

[29] J. Tersoff, Phys. Rev. B **39**, 5566 (1989).

[30] D. W. Brenner, Phys. Rev. B **42**, 9458 (1990).

[31] W. K. Park and S. C. Park, J. Mol. Struct. **630**, 215 (2003).

[32] E. Hayakawa, F. Khanom, T. Yoshifuku, S. Shimokawa, A. Namiki, and T. Ando, Phys. Rev. B **65**, 033405 (2001).

[33] F. Khanom, A. Aoki, F. Rahman, and A. Namiki, Surf. Sci. **536**, 191 (2003).

[34] T. Ohira, O. Ukai, and M. Noda, Surf. Sci. **458**, 216 (2000).

[35] R. Biswas, B. C. Pan, and Y. Y. Ye, Phys. Rev. Lett. **88**, 205502 (2002).

[36] B. Pan and R. Biswas, J. Non-Cryst. Solids **333**, 44 (2004).

[37] R. Biswas and B. Pan, *Simulation of Realistic Core-Shell Silicon Nanowires*, in Materials Research Society Symposium Proceedings, Vol. 910 (Materials Research Society, Warrendale, PA, 2006), pp. 15–20.

[38] G. Panzarini and L. Colombo, Phys. Rev. Lett. **73**, 1636 (1994).

[39] Y. S. Su and S. T. Pantelides, Phys. Rev. Lett. **88**, 165503 (2002).

[40] C. Krzeminski, Q. Brulin, V. Cuny, E. Lecat, E. Lampin, and F. Cleri, J. Appl. Phys. **101**, 123506 (2007).

[41] W. Barvosa-Carter, M. J. Aziz, A.-V. Phan, T. Kaplan, and L. J. Gray, J. Appl. Phys. **96**, 5462 (2004).

[42] M. J. Aziz, P. C. Sabin, and G.-Q. Lu, Phys. Rev. B **44**, 9812 (1991).

[43] K. S. Stevens and N. M. Johnson, J. Appl. Phys. **71**, 2628 (1992).

[44] T. Rajendra and B. Parthapratim, Phys. Status Solidi (A) **207**, 609 (2010).

[45] G. T. Barkema and N. Mousseau, Phys. Rev. B **62**, 4985 (2000).

[46] A. Mattoni and L. Colombo, Phys. Rev. B **69**, 045204 (2004).

[47] M. Cogoni, A. Mattoni, B. P. Uberuaga, A. F. Voter, and L. Colombo, Appl. Phys. Lett. **87**, 191912 (2005).

[48] S. Mirabella, A. Coati, D. De Salvador, E. Napolitani, A. Mattoni, G. Bisognin, M. Berti, A. Carnera, A. V. Drigo, S. Scalese *et al.*, Phys. Rev. B **65**, 045209 (2002).

[49] A. Mattoni, F. Bernardini, and L. Colombo, Phys. Rev. B **66**, 195214 (2002).

[50] N. Budini, P. Rinaldi, J. Schmidt, R. Arce, and R. Buitrago, Thin Solid Films **518**, 5349 (2010).

[51] S. Ahrenkiel, A. Mahan, D. Ginley, and Y. Xu, Mater. Sci. Eng.: B **176**, 972 (2011).